ORGANIC CHEMISTRY FRONTIERS

RESEARCH ARTICLE

View Article Online
View Journal

Cite this: DOI: 10.1039/d6qo00080k

Cobalt-catalyzed C–H annulation of aliphatic amides with maleimides: chemodivergent (4 + 1) and (3 + 2) pathways

Celia Sánchez-González,[a] Juan C. Carretero,[a,b] Inés Alonso,[*a,b] Nuria Rodríguez[*a,b] and Javier Adrio[*a,b]

Received 21st January 2026,
Accepted 17th February 2026

DOI: 10.1039/d6qo00080k

rsc.li/frontiers-organic

Chemodivergent C–H annulation of aliphatic amides with maleimides has been achieved under cobalt-catalysis, enabling access to distinct (4 + 1) and (3 + 2) outcomes. These protocols, utilizing a readily available Co^{II}-catalyst, deliver a powerful strategy for the synthesis of a diverse range of spiro-γ-lactams (spiro-pyrrolidin-2-ones) and bicyclic pyrrolidin-2,5-diones. The combination of DFT and experimental studies provides mechanistic insight into both processes, revealing the origins of their diastereo- and chemoselectivity.

Introduction

The synthesis of complex organic compounds conventionally relies on controlling the reactivity of different functional groups within the substrate's structure.[1] Extending this paradigm to the selective direct functionalization of unreactive C–H bonds has become a central quest in modern synthetic chemistry.[2] Particularly compelling is the development of chemodivergent C–H transformations, a promising strategy for rapidly generating molecular diversity from common starting materials.[3] However, such modular approaches remain highly challenging due to the inherent complexity of controlling multiple competing reaction pathways.

Among C–H functionalization strategies, transition-metal-catalyzed C(sp^3)–H annulation stands out as a particularly powerful platform for constructing saturated carbo- and heterocyclic frameworks.[4] The success of this approach critically depends on the design of an appropriate directing group (DG) to promote selective activation of otherwise inert C(sp^3)–H bonds, typically *via* formation of a key metallacycle intermediate. Subsequent annulation from this intermediate provides direct access to complex cyclic architectures from readily available alkyl substrates. This mechanistic framework, when combined with careful tuning of catalyst and conditions, opens exciting opportunities for achieving chemodivergent outcomes in C(sp^3)–H functionalization.[5]

Traditionally, C(sp^3)–H annulation processes have been conducted using noble metal catalysts,[4a] with palladium standing out as the most widely employed.[6] However, interest in earth-abundant 3d metals[7] has shifted focus toward cobalt,[8,9] which offers distinct reactivity and site-selectivity. The diverse coordination geometries and electronic configurations accessible to cobalt complexes enable activation modes and bond-forming pathways that are often inaccessible to noble-metal systems, positioning cobalt as a valuable complementary platform for expanding the scope and strategic utility of C(sp^3)–H annulation chemistry.

High-valent cobalt complexes, in particular, have garnered increasing attention in DG-assisted C(sp^3)–H activation due to their distinctive electronic properties and redox flexibility.[10] Notably, simple Co^{II}-precursors in combination with 8-aminoquinoline (8-AQ) as a bidentate DG have proven highly effective for β-C(sp^3)–H functionalization of carbonyl compounds, enabling a broad range of oxidative annulation reactions. These include intramolecular C–N bond-forming cyclization,[11] and formal cycloaddition pathways such as intramolecular alkene coupling,[12] intermolecular coupling with alkynes,[13] and oxidative C(sp^3)–H/N–H carbonylation of aliphatic amides with carbon monoxide.[14] Nevertheless, intermolecular β-C(sp^3)–H coupling with alkenes has, to the best of our knowledge, not yet been achieved.

Motivated by this unmet challenge, we turned our attention to maleimides, highly electrophilic olefins widely used as coupling partners in transition-metal-catalyzed C–H functionalization reactions.[15] Their application in annulation processes, however, remains comparatively underdeveloped. This limitation largely arises from competing side reactions, including alkenylation *via* E2-type elimination[16] and alkylation

[a]*Dpto. de Química Orgánica, Facultad de Ciencias, Universidad Autónoma de Madrid (UAM), Cantoblanco 28049, Madrid, Spain. E-mail: ines.alonso@uam.es, n.rodriguez@uam.es, javier.adrio@uam.es*
[b]*Institute for Advanced Research in Chemical Sciences (IAdChem) and Center for Innovation in Advanced Chemistry (ORFEO-CINQA) UAM, 28049 Madrid, Spain*

through protodemetallation,[17] which often compromise reaction efficiency and selectivity. Nonetheless, effective strategies have been devised to address these issues, particularly in the realm of C(sp^2)–H activation.[18] A remarkable example is the work of Jeganmohan *et al.*, who reported a Co^{II}-catalyzed (4 + 1) spirocyclization of aromatic amides with maleimides directed by 8-AQ (Scheme 1a).[19] Years later, Shi *et al.* developed an asymmetric variant using a Co^{II}/chiral spirophosphoric acid catalytic system that enables the synthesis of chiral spiro-γ-lactams in good yields and excellent enantioselectivities.[20] More recently, the merger of cobalt-catalyzed C(sp^2)–H activation with electrochemical and visible-light photocatalytic techniques has enabled access to related spirocyclic scaffolds.[21]

In contrast, the use of maleimides in C(sp^3)–H annulations remains underdeveloped. To date, only a few examples based on Pd catalysis have been reported. M. Jeganmohan *et al.* disclosed an oxidative spirocyclization of 2,2-dimethyl-substituted alkyl nosylamides *via* β-C(sp^3)–H activation (Scheme 1b).[22a] More recently, the same group reported a Pd-catalysed spirocyclisation of substituted amino acids with maleimides through γ-C(sp^3)–H bond activation, further highlighting the potential of this transformation.[22b] Alternatively, Yu's group described a Pd-catalyzed (3 + 2) annulation of *gem*-dimethyl-containing amide derivatives enabled by dual C(sp^3)–H bond activation (Scheme 1b).[23,24] In this system, only a limited number of secondary NH-alkyl amides were tested.

Building on these precedents and leveraging the distinctive reactivity profile of cobalt catalysis, we sought to develop a strategy for the annulation of secondary aliphatic amides *via* β-C(sp^3)–H activation with maleimides. Through fine-tuning of the reaction conditions, we uncovered two complementary cobalt-catalyzed pathways: (i) a sequential C(sp^3)–H activation followed by oxidative (4 + 1) spirocyclization, and (ii) a (3 + 2) annulation proceeding through dual C(sp^3)–H activation involving two distinct methyl groups (Scheme 1c). Both transformations occur without altering the inherent nature of the amide DG, highlighting the power of reaction design in expanding the synthetic utility of cobalt-catalyzed C–H functionalization. This chemodivergence prompted further investigation into the reaction parameters and underlying mechanistic features, as discussed below.

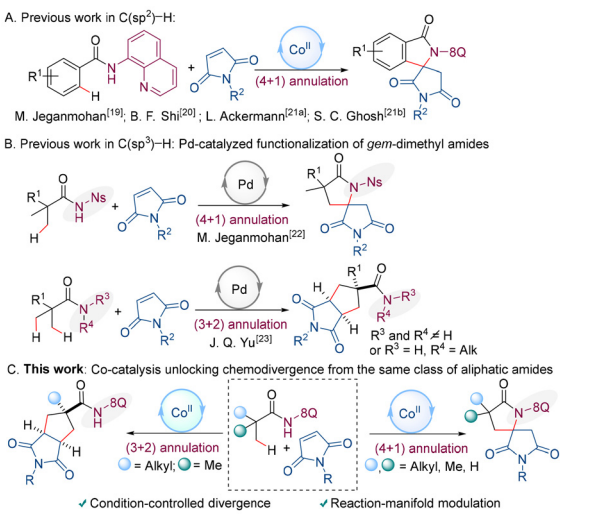

Scheme 1 Maleimides as coupling partners in C–H functionalization.

Results

Optimization of reaction conditions for the annulation processes

To elucidate the reaction conditions, we selected *N*-(quinoline-8-yl)pivalamide (**1a**) and *N*-phenyl maleimide (**2a**) as a model system. Employing Co(OAc)$_2$·4H$_2$O (15 mol%) as catalyst, Ag$_2$CO$_3$ (4.0 equiv.) as oxidant, and NaOPiv (0.5 equiv.) as basic additive in DCE at 140 °C for 24 h, the spiro-γ-lactam **3aa** was isolated in an excellent 87% yield (Table 1, entry 1) (see the SI for full optimization studies, including a detailed evaluation of diverse DGs).

Strikingly, replacement of NaOPiv with PivOH lowered the yield of **3aa** and unveiled the formation of the (3 + 2) annulation product **4aa** with excellent diastereoselectivity (13%, d.r. > 20 : 1, entry 2). Motivated by this result, we next sought to assess the feasibility of a chemodivergent strategy through systematic variation of the reaction parameters. Attempts to favor the (3 + 2) pathway with substrate **1a**, however, were unsuccessful (see SI). We therefore investigated whether subtle structural modifications of the substrate could bias the reaction toward the alternative (3 + 2) annulation manifold. Exchange of **1a** with α,α′-dimethylbutanamide **1b** delivered **3ba** and **4ba** in 24% and 20% yield, respectively (entry 3). While **3ba** was obtained as a 1.1 : 1 diastereomeric mixture, **4ba** was formed as single diastereomer.

Table 1 Evaluation of reaction conditions[a]

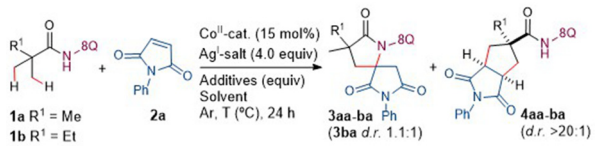

Entry	1	Co^{II}-cat.	Ag^{I}-salt	Additive	3 [b] (%)	4 [b] (%)
1	**a**	**Co(OAc)$_2$·4H$_2$O**	**Ag$_2$CO$_3$**	**NaOPiv**	**90 (87)**[c]	**n.d.**
2	a	Co(OAc)$_2$·4H$_2$O	Ag$_2$CO$_3$	PivOH	44	13
3	b	Co(OAc)$_2$·4H$_2$O	Ag$_2$CO$_3$	PivOH	24	20
4	b	Co(OAc)$_2$·4H$_2$O	Ag$_2$O	PivOH	12	20
5[d]	b	Co(OAc)$_2$	Ag$_2$O	PivOH	17	35
6[d,e]	b	Co(OAc)$_2$	Ag$_2$O	PivOH	18	47
7[d,e,f]	**b**	**Co(OAc)$_2$**	**Ag$_2$O**	**PivOH**	**15 (12)**[c]	**63 (63)**[c]
8	b	Co(OAc)$_2$·4H$_2$O	Ag$_2$CO$_3$	NaOPiv	63 (61)[c]	8 (7)[c]

[a] *Reaction conditions*: **1** (0.1 mmol, 1.0 equiv.), **2a** (0.25 mmol, 2.5 equiv.), Co(OAc)$_2$·4H$_2$O (15 mol%), Ag$_2$CO$_3$ (0.4 mmol, 4.0 equiv.), NaOPiv (0.05 mmol, 0.5 equiv.), DCE (0.5 mL), 140 °C, 24 h. [b] Yield determined by ^{1}H NMR using 1,3,5-trimethoxybenzene as internal standard. [c] Isolated yield. [d] 120 °C. [e] DCE: *n*-hexane (1 : 0.5) (0.13 M). [f] Adding pyridine-3-sulfonic acid (0.07 mmol, 0.7 equiv.). n.d. = not detected. DCE = 1,2-dichloroethane.

A slight decrease in overall yield, accompanied by improved selectivity toward **4ba**, was observed when Ag_2CO_3 was replaced with Ag_2O (entry 4). The use of anhydrous $Co(OAc)_2$ combined with a reduced reaction temperature of 120 °C markedly increased the conversion, preserving the selectivity in favour of **4ba** (**3ba** : **4ba** = 1 : 2, entry 5). Further improvement in the yield of **4ba** was achieved using a mixture of DCE/*n*-hexane (1 : 0.5) as solvent (entry 6), likely by modulating the solubility or aggregation state of the catalytic species. Finally, addition of pyridine-3-sulfonic acid (0.7 equiv.) led to an increase in both yield and selectivity for the (3 + 2) pathway, affording **3ba** and **4ba** in 12% and 63% isolated yields, respectively (entry 7).

Importantly, under the previously optimized conditions for the formation of the (4 + 1) product ($Co(OAc)_2{\cdot}4H_2O/Ag_2CO_3$/NaOPiv/140 °C), substrate **1b** selectively afforded the spiro-γ-lactam **3ba** in 61% isolated yield (entry 8).[25] This result validates the chemodivergent nature of the Co-catalyzed annulation.

Exploring the structural versatility of the chemodivergent methodology

To further probe the chemodivergent potential of both annulation pathways, we examined their generality across structurally varied substrates. We began by evaluating the $Co(OAc)_2{\cdot}4H_2O/Ag_2CO_3$/NaOPiv catalytic system for the selective synthesis of (4 + 1) spiro-γ-lactam derivatives **3** (Scheme 2). A series of α,α-disubstituted propanamides (**1c–1i**) were subjected to the optimized conditions, delivering the corresponding (4 + 1) products **3ca–3ia** in 43–74% yield with an approximate 1 : 1 diastereomeric ratio. The individual diastereomers could be readily isolated by column chromatography. The transformation proved tolerant to various alkyl chain lengths and functional groups, including trifluoromethyl, halogens, methoxy, aromatic moieties, and amides. As indicated in the scheme, under these reaction conditions, the alternative (3 + 2) annulation products (**4**) were obtained in yields of less than 15% in all cases. α-Monosubstituted propanamides were also adequate substrates, although only moderate yields of the corresponding spiro-γ-lactams were obtained (**3ja**: 50%; **3ka**: 30%), with substantial recovery of unreacted starting materials. Simple propanamide **1l** afforded **3la** in 12% yield. Remarkably, 1-methylcycloalkyl-1-carboxamides smoothly participated in the reaction to give the corresponding (4 + 1) annulation products in good yields (**3ma–3oa**, 50–70%). Methylene β-C–H bond functionalization of the cyclopropane-derivative **1p** also occurred, affording **3pa** in 31% (d.r. 1.2 : 1). In addition, acrylamide derivative **1q** underwent preferential β-C(sp^2)–H bond functionalization over the β-methyl C(sp^3)–H bond, affording **3qa** in an excellent 95% yield. Expanding the substrate scope further, a variety of maleimides were successfully tested, with no substantial influence from their *N*-substituents. To evaluate the scalability of the process, a 1.0 mmol scale reaction of **1r** and **2a** was conducted under standard conditions and the desired product **3ra** was provided in 50% yield. Subsequently, the removal of the methoxyquinolinyl group from **3ra** gave **5** in 72% yield.

Subsequently, the $Co(OAc)_2/Ag_2O$/PivOH catalytic system was evaluated for its efficiency in the selective synthesis of bicyclic pyrrolidin-2,5-dione derivatives **4** (Scheme 3). α,α-Disubstituted propanamides (**1c–1h**) furnished the corresponding (3 + 2) annulation products (**4ca–4ha**) in moderate to good yields (30–90%) and with an outstanding diastereoselectivity (d.r. > 20 : 1). Overall, the major diastereomers in all cases showed *cis* relationship between the imide group and the amide DG. It is important to emphasize that previous Pd-catalyzed procedures typically produced mixtures of diastereomers.[23] Alternative (4 + 1) annulation products **3** were obtained

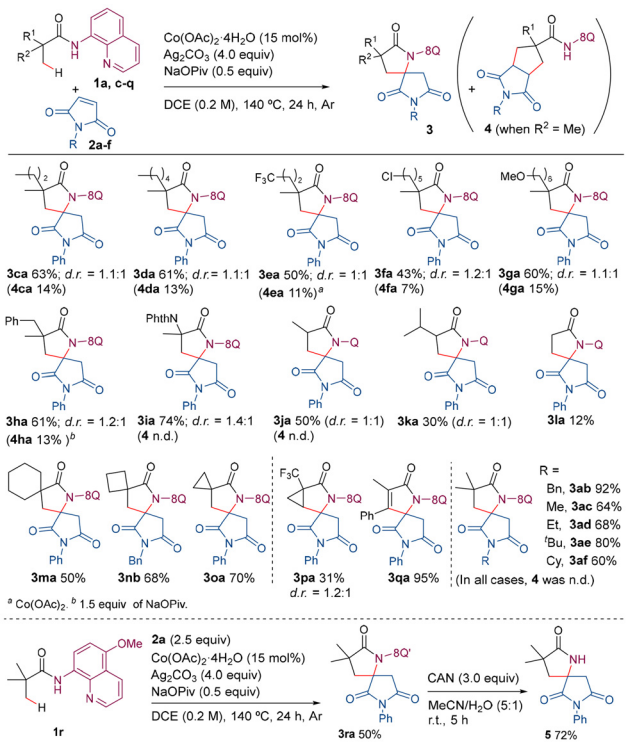

Scheme 2 (4 + 1) annulation strategy: structural versatility.

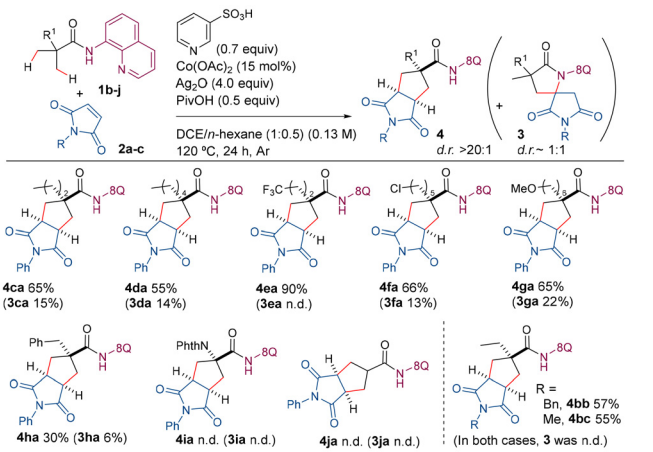

Scheme 3 (3 + 2) annulation strategy: structural versatility.

in yields of less than 22% in all cases. Unfortunately, propanamides **1i** and **1j** proved unreactive under the standard conditions. The reaction also tolerated variation in the *N*-substituent of the maleimide, delivering the desired products **4bb** and **4bc** in 57% and 55% yield, respectively. Unfortunately, maleimides bearing strongly electron-withdrawing *N*-substituents such as Boc or Ac were found to be unstable under the reaction conditions and therefore did not afford any annulation products.

Finally, to expand the structural scope of the (3 + 2) annulation involving a dual *gem*-C–H activation process, we examined the reaction of 1-methylcyclohexyl-1-carboxamide (**1m**). Remarkably, this substrate smoothly underwent the transformation to give the corresponding (3 + 2) annulation product **6** in 31% yield, along with 15% of the (4 + 1) spirocyclization product (**3ma**). The formation of **6** demonstrates the capability of our catalytic system to engage in formal (3 + 2) cycloaddition involving activation of both methyl and methylenic C–H bonds, as illustrated in Scheme 4.

Experimental insights into the reaction mechanism

At this point, challenged by the chemodivergency achieved by fine-tuning the reaction conditions, we decided to investigate the mechanism behind each of these transformations. We began our study focusing on the (4 + 1) annulation strategy (Scheme 5a). The reaction of **1a** with **2a** was performed in the presence of AcOH-d_4 (3.0 equiv.) under the optimized conditions: $Co(OAc)_2{\cdot}4H_2O/Ag_2CO_3$/NaOPiv/140 °C. Analysis at an intermediate time point (5 h) revealed no deuterium incorporation in the recovered starting material **1a**, suggesting that activation of the C(sp^3)–H bond may be irreversible. Similarly, no H/D exchange was observed in **1a** when the reaction was performed in the absence of **2a** (data not shown; see SI). In contrast, H/D exchange occurred diastereoselectively at a methylene C–H bond of the succinimide moiety in **3aa-D** (Scheme 5a). Although the origin of this selectivity was not yet understood;[26] it was anticipated to be a key feature in supporting a mechanistic hypothesis and would be therefore addressed in subsequent DFT studies.

With respect to the (3 + 2) strategy, we performed the same set of experiments, this time using **1b** as the starting material (Scheme 5b). Analysis of the crude reaction mixture after 5 h revealed no deuterium incorporation either in **1b** or in the reaction product **4ba**. Therefore, we assumed that the C–H activation was likely irreversible.

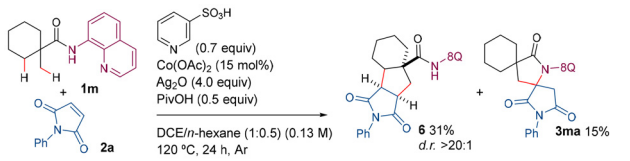

Scheme 4 Cobalt-catalyzed (3 + 2) annulation reaction engaging methyl and methylene C–H bonds.

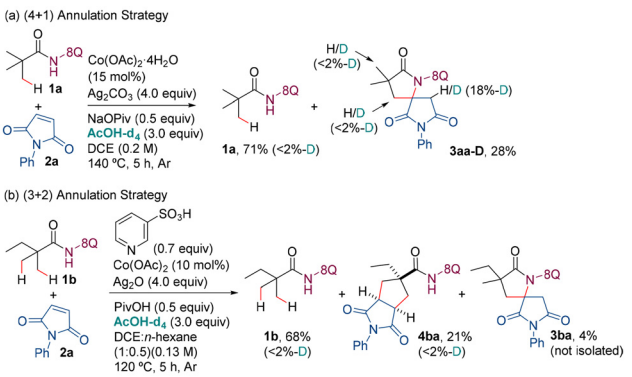

Scheme 5 H/D scrambling experiments.

Theoretical studies toward mechanistic elucidation

In line with these experimental findings, we next performed DFT studies (M06-L level) using **1a** as a model structure for simplicity.

Based on previous reports and in our own experience,[27,13a] we assumed that **1a** initially coordinates to $Co(OAc)_2$, forming a Co^{II} complex which, upon *in situ* oxidation by Ag^I, evolves into a stable monomeric Co^{III} species. Subsequently, C(sp^3)–H activation *via* an acetate-assisted concerted-metalation deprotonation (CMD) mechanism furnishes cobaltacycle **IM1**, retaining AcOH coordinated to the metal (Fig. 1). Displacement of AcOH by maleimide **2a** leads to the formation of intermediate **IM2** (9.0 kcal mol^{-1}),[28] which precedes the 1,2-migratory insertion of the maleimide into the C–Co bond. This key step results in the exergonic formation of the bicyclic intermediate **IM3** (−10.5 kcal mol^{-1}). From **IM3**, the reaction landscape splits into multiple mechanistic trajectories, providing a possible explanation of the chemodivergent reactivity achieved.

First, we focused on the (4 + 1) annulation strategy (Fig. 1). Consistent with previously proposed mechanisms,[20] intermediate **IM3** could undergo an acetate-assisted E2-type elimination to yield the anionic Heck-type Co^I species **IM4**, which lies at −24.4 kcal mol^{-1} in its single state (**IM4-s**). Calculations indicate that a subsequent direct 1,2-migratory insertion of the double bond into the N–Co bond is highly unfavorable [**IM4-s** → **IM5** (−10.8 kcal mol^{-1}) → **TS3** (34.4 kcal mol^{-1})]. However, considering the tendency of $Co^I(d^8)$ to have triplet ground states, particularly stable in square planar or distorted octahedral geometries, we decided to investigate both singlet and triplet electronic states of intermediates in which Co center changes its oxidation state from formal +3 to formal +1. A comparison of the singlet and triplet electronic states of **IM4** revealed that the triplet state is more stable than the singlet (**IM4-t**, −27.8 kcal mol^{-1}, shown in orange). From **IM4-t**,[29] the reaction then likely proceeds *via* an AcOH-mediated intramolecular aza-Michael addition, which takes place through **TS4-t** (11.2 kcal mol^{-1}), leading to **IM6-t** (6.2 kcal mol^{-1}). In this intermediate, the C–N bond has formed and the cobalt center coordinates to the α-carbon of the other carbonyl group of the imide moiety [*d*(C–Co): 2.25 Å]. For benchmarking, the

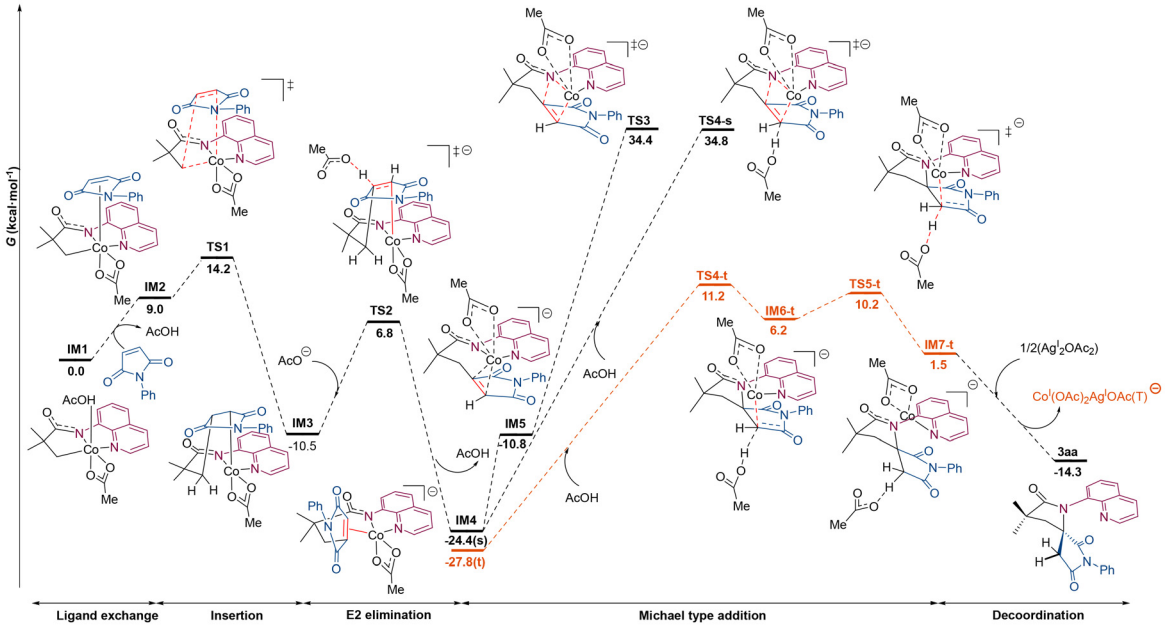

Fig. 1 Energy profile for the formation of isomer **3aa** *via* Michael type addition in DCE [M06-L_{SMD}/6-311+G(2df,2p) (C,H,N,O), SDD (Co,Ag)//M06-L_{SMD}/6-31G(d) (C,H,N,O), LANL2DZ(f) (Co,Ag) at 298 K].

pathway from **IM4-s** was also examined, but proved energetically unfeasible, with the lowest-lying calculated transition state (**TS4-s**) at 34.8 kcal mol^{-1}.

From **IM6-t**, protodemetallation by AcOH completes the annulation, affording the Co^{I} complex **IM7** (1.5 kcal mol^{-1}), in which the resulting (4 + 1) product **3aa** remains coordinated to the metal through the quinoline nitrogen. The stereoselectivity of this protonation step accounts for the selectivity observed in the earlier H/D experiment (Scheme 5a). **3aa** is finally released (ΔG = −14.3 kcal mol^{-1}) *via* displacement of [Co^{I}(OAc)$_2$Ag^{I}OAc]$^{-}$-*t* facilitated by Ag^{I} complexes, with [Ag$_2$(OAc)$_2$] used as a model.

Nonetheless, due to the sequence of bond formation and the spatial orientation of the maleimide moiety within the cobalt complex **IM6-t**, this mechanism alone can only account for the formation of one of the diastereomers observed in the reactions with prochiral propanamides (**1b–k**). Therefore, we search for an alternative mechanistic proposal to rationalize the formation of the second isolated diastereomer.[30]

In this search, our investigations uncovered the complementary mechanistic pathway illustrated in Fig. 2. This pathway suggests a second role for acetate: in addition to promoting an acetate-assisted E2-type elimination from **IM3** to generate the anionic Heck-type Co^{I} species (Fig. 1), acetate can also coordinate to **IM3**, facilitating its conversion to the anionic Co^{III} intermediate **IM8** (−14.8 kcal mol^{-1}). Such dual behavior highlights the versatility of acetate in steering the reaction along different mechanistic routes. From **IM8**, to rationalize the formation of the other isomer **3aa′** (considered with the opposite configuration in the spirocyclic carbon for a fixed arrangement of the methyl groups), an AcOH-mediated protodemetalation step is proposed, affording **IM9** (−6.8 kcal mol^{-1}), in which the resulting γ-alkylated propanamide remains coordinated to the cobalt center through the 8-AQ DG. Subsequently, γ-C–H activation of the alkylated propanamide *via* transition state **TS7** (19.6 kcal mol^{-1}) furnishes intermediate **IM10** (−2.8 kcal mol^{-1}), with AcOH still bound to the metal. This intermediate readily evolves to **IM11** (−21.2 kcal mol^{-1}) upon release of the AcOH unit. A subsequent ligand rearrangement to **IM12** (−20.7 kcal mol^{-1}), which probably involves decoordination, change of conformation and recoordination of N atoms, would position the system optimal for C–N bond formation, which occurs *via* transition state **TS8-s** (21.9 kcal mol^{-1}), giving rise to the Co^{I} intermediate **IM13-s** (13.6 kcal mol^{-1}). Calculations reveal that this reductive elimination step is much more favored when considering the triplet ground state of the Co^{I} species involved, lowering both the energy barrier for the reductive elimination and stabilizing the reductive elimination product **IM13-t** (−8.5 kcal mol^{-1}).

Building upon the mechanistic insights discussed above, it becomes evident that both reaction pathways should be considered to comprehensively account for the formation of the two observed isomers **3aa** and **3aa′**. The computed activation energy barriers for the key steps in both pathways (to reach **TS4-t** and **TS6** respectively) are comparable, explaining the experimentally observed lack of diastereoselectivity with prochiral α-substituted and α,α′-disubstituted propanamides (**1b–k**).

Next, we examine the (3 + 2) pathway, which, as shown in Fig. 3, originates from the same anionic Co^{III} intermediate **IM8** (−14.8 kcal mol^{-1}). A conformational change from **IM8** would lead to **IM14** (−4.8 kcal mol^{-1}), in which a second methyl group is positioned for a subsequent C(sp^3)–H activation [*d*(Co–H): 1.89 Å]. This step proceeds *via* an acetate-

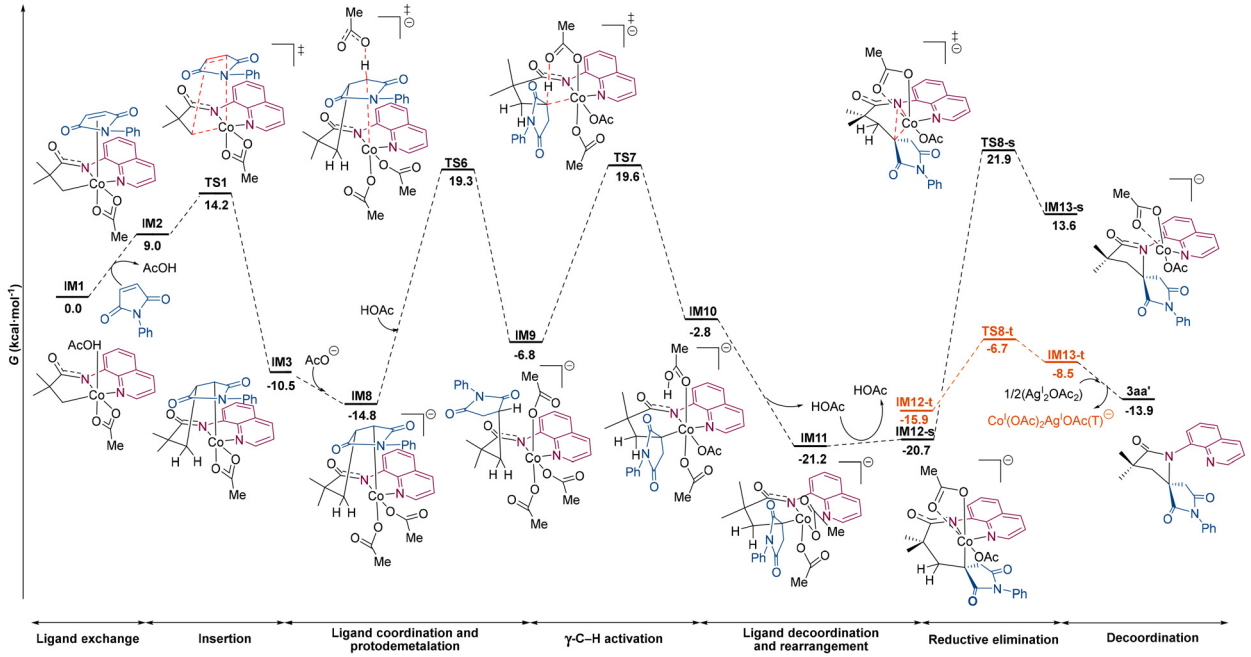

Fig. 2 Energy profile for the formation of isomer **3aa′** *via* γ-C–H activation in DCE [M06-L_{SMD}/6-311+G(2df,2p) (C,H,N,O), SDD (Co,Ag)//M06-L_{SMD}/6-31G(d) (C,H,N,O), LANL2DZ(f) (Co,Ag) at 298 K].

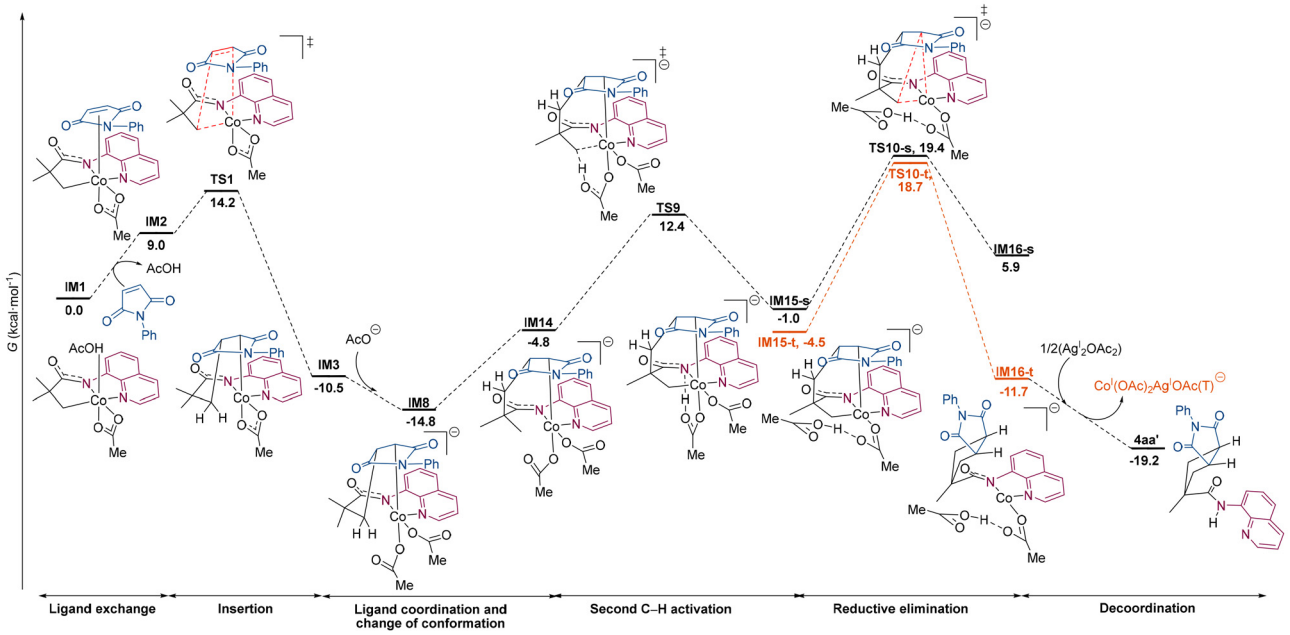

Fig. 3 Energy profile for the Co-catalyzed (3 + 2) annulation through sequential C–H activation in DCE [M06-L_{SMD}/6-311+G(2df,2p) (C,H,N,O), SDD (Co,Ag)//M06-L_{SMD}/6-31G(d) (C,H,N,O), LANL2DZ(f) (Co,Ag) at 298 K].

assisted CMD mechanism through transition state **TS9** (12.4 kcal mol^{-1}), affording the cobaltacycle **IM15-s** (−1.0 kcal mol^{-1}), with AcOH remaining coordinated and forming a hydrogen bond with the amide nitrogen.

Nonetheless, although this route appears chemically reasonable and aligns with established precedents involving sequential C–H activations, it ultimately proves unlikely as it leads to the formation of the unobserved diastereomer **4aa′** featuring a *trans* relationship between the imide and the DG.[31] Crucially, the second C–H activation is reversible, a key feature that could help rationalize why the reaction does not proceed through this pathway. Advancing beyond this point would

require C–C bond formation *via* **TS10-s** (19.4 kcal mol^{-1}), leading to **IM16-s** (5.9 kcal mol^{-1}). However, the barrier for this step exceeds that for the reverse C–H activation, rendering the overall process kinetically disfavored.

Even considering the triplet state of the cobalt species does not rescue this mechanism: while C–C bond formation [**IM15-t** (−4.5 kcal mol^{-1}) → **TS10-t** (18.7 kcal mol^{-1}) → **IM16-t** (−11.7 kcal mol^{-1})] becomes irreversible and thermodynamically more favorable than in the singlet manifold, it would still be less favored than the reverse reaction. These findings underscore the limitations of this mechanistic pathway and highlight the necessity of considering other routes to account for the observed stereochemical outcome.

As illustrated in Fig. 4, an alternative scenario involves a ligand reorganization from **IM8** *via* coordination/decoordination of AcOH to form **IM17** (−5.4 kcal mol^{-1}). This rearrangement defines the stereochemical course of reaction by positioning the alternate methyl group for C(sp^3)–H metalation *via* **TS11** (12.0 kcal mol^{-1}), affording **IM18** (−14.2 kcal mol^{-1}), with AcOH remaining bound to the Co center. Subsequent liberation of AcOH yields the more stable intermediate **IM19-s** (−19.9 kcal mol^{-1}). From this point, the C–C bond formation *via* the lowest-energy transition state **TS12-s** (10.0 kcal mol^{-1}), leads reversibly to the Co^{I} species **IM20-s** (9.2 kcal mol^{-1}), which undergoes conformational reorganization to form **IM21-s** (−1.3 kcal mol^{-1}). Notably, considering the triplet manifold for this last transformation renders the C–C bond-forming step both irreversible and thermodynamically more favorable: [**IM19-t** (−11.9 kcal mol^{-1}) → **TS12-t** (9.9 kcal mol^{-1}) → **IM20-t** (−16.5 kcal mol^{-1}) → **IM21-t** (−19.6 kcal mol^{-1})]. Finally, the presence of acid to release the catalyst from intermediate **IM21**, in which it is still coordinated to the nitrogen atoms of the amide and quinoline, could support the relatively more acidic conditions required to obtain (3 + 2) selectivity. This mechanistic route, therefore, accounts for the formation of the experimentally observed **4aa** diastereomer, providing a stereochemically consistent and energetically favorable pathway.

Mechanistic hypotheses: proposed catalytic cycles and main features

To summarize the mechanistic information and facilitate a clearer comparison of all competing processes, the final proposed mechanisms are presented in the cycles below: Scheme 6 illustrates both operating mechanisms for the (4 + 1) process, whereas Scheme 7 outlines the proposed pathway for the formation of the (3 + 2) adduct.

From this overall picture, the following key conclusions can be drawn:

(a) Both the (4 + 1) and (3 + 2) pathways begin with AQ deprotonation by Co^{II}-coordinated carboxylates, forming a Co^{II} complex that is oxidized *in situ* by Ag^{I} to a stable Co^{III} species. C(sp^3)–H activation *via* an acetate-assisted CMD mechanism yields cobaltacycle **IM1**, which, upon maleimide coordination and 1,2-migratory insertion into the C–Co bond, forms the bicyclic intermediate **IM3**.

(b) In the (4 + 1) process (Scheme 5), **IM3** either undergoes E2-elimination followed by aza-Michael addition (Path A) or rearranges evolving *via* protodemetalation, γ-C–H activation and C–N bond formation (Path B), both ultimately delivering the annulation product and regenerating the catalyst through Ag^{I}-mediated product displacement and reoxidation. The coexistence of these two routes explains the observed lack of diastereoselectivity with prochiral substrates.

(c) In the (3 + 2) process (Scheme 7), the diastereoselective formation of product **4** from **IM3** could be explained by a

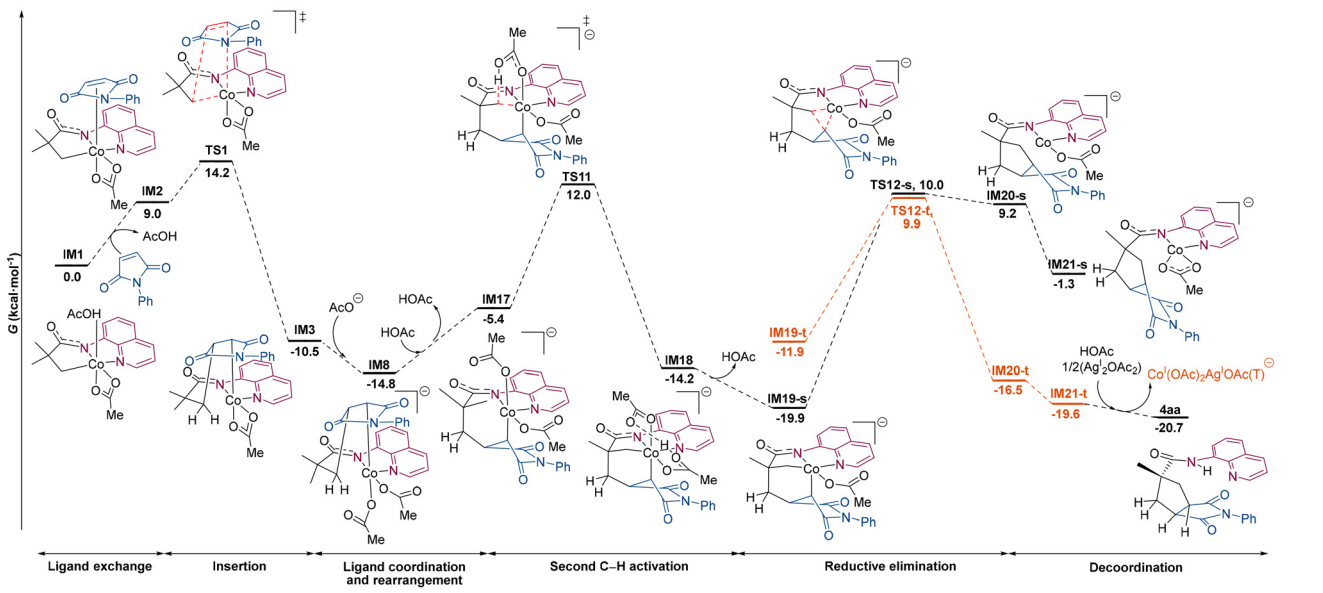

Fig. 4 Energy profile for the Co-catalyzed (3 + 2) annulation for the formation of the observed diastereomer **4aa** in DCE [M06-L$_{SMD}$/6-311+G (2df,2p) (C,H,N,O), SDD (Co,Ag) //M06-L$_{SMD}$/6-31G(d) (C,H,N,O), LANL2DZ(f) (Co,Ag) at 298 K].

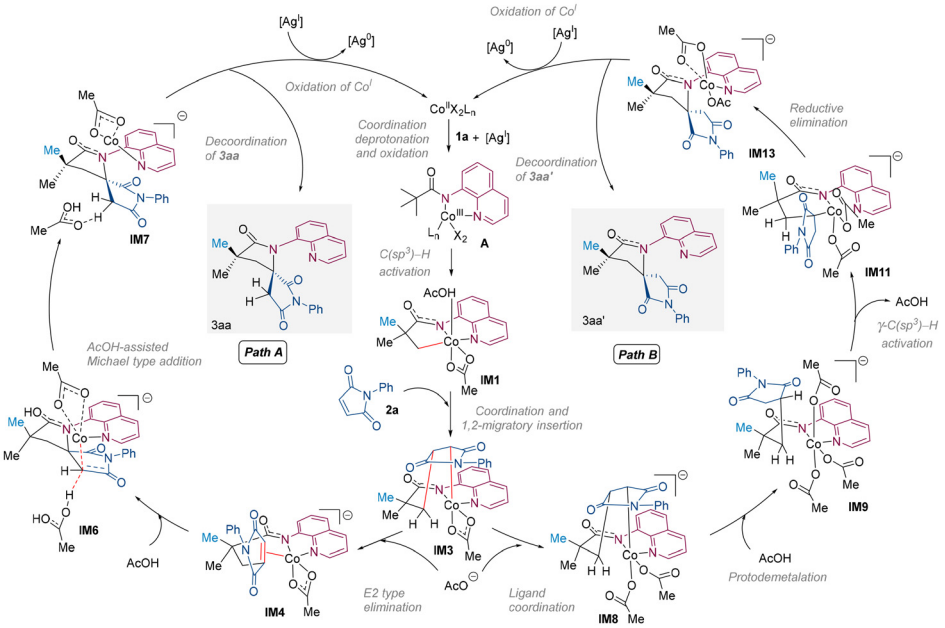

Scheme 6 Global (4 + 1) annulation process.

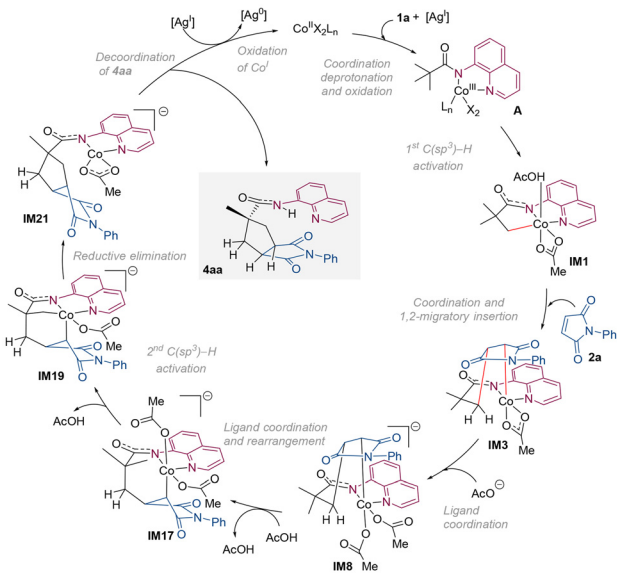

Scheme 7 (3 + 2) annulation process.

ligand reorganization, enabling a dual C(sp^3)–H activation involving two distinct methyl groups.

(d) Based on the critical barriers for both cyclization processes shown in Fig. 1–4, it can be deduced that the higher energy demand for the (4 + 1) annulation process can be correlated with the higher temperature required in this case [140 °C compared to 120 °C for the (3 + 2) process]. On the other hand, the presence of water, which is essential for promoting the (4 + 1) annulation process, could contribute to increasing the polarity of the medium, facilitating the protodemetalation reactions present in this route. Therefore, temperature and the presence of water play a crucial role in achieving selectivity, which is also modulated by the use of controlled acidic conditions or certain ligands, such as pyridine-3-sulfonic acid, by facilitating protonation/deprotonation events and stabilizing spin-state-dependent intermediates.

Conclusions

In summary, a chemodivergent 8-AQ-assisted cobalt-catalyzed annulation of aliphatic amides with maleimides has been successfully achieved employing Co(OAc)$_2$ as a simple Co^{II}-catalyst precursor. By fine tuning of the reaction conditions, selective control can be exerted to enable either a sequential C(sp^3)–H activation followed by (4 + 1) spirocyclization, or a (3 + 2) annulation involving the dual activation of two distinct C(sp^3)–H bonds on different carbon centers. The chemo- and stereoselectivity that have been achieved can be rationalized by the intermediates identified by DFT calculations.

Taking all of this into account, this work demonstrates cobalt catalysis as a versatile platform for chemodivergent processes, providing new mechanistic insights that differentiate cobalt from heavier transition metals. These findings pave the way for more effective and innovative cobalt-based catalytic strategies in the future.

Author contributions

The manuscript was written through contributions of all authors. All authors have given approval to the final version of the manuscript.

Conflicts of interest

There are no conflicts to declare.

Data availability

The data supporting this article have been included as part of the supplementary information (SI). Supplementary information: NMR spectra, further experimental and computational details. See DOI: **https://doi.org/10.1039/d6qo00080k**.

Acknowledgements

We thank FEDER/Ministerio de Ciencia, Innovación y Universidades–Agencia Estatal de Investigación (Grant PID2021-124853NB-100) for financial support. C. S.-G. thanks MICIU for a FPU predoctoral fellowship (FPU21/04031). We also thank the Centro de Computación Científica at the Universidad Autónoma de Madrid for their generous allocation of computer time. We thank S. Diaz-Tendero for his advice in DFT calculations.

References

1 *Name Reactions for Functional Group Transformations*, ed. J. J. Li and E. J. Corey,Wiley, Hoboken, NJ, 2007.

2 (*a*) M. C. White, Adding aliphatic C–H bond oxidations to synthesis, *Science*, 2012, **335**, 807–809; (*b*) J. Wencel-Delord, T. Dröge, F. Liu and F. Glorius, Towards mild metal-catalyzed C–H bond activation, *Chem. Soc. Rev.*, 2011, **40**, 4740–4761; (*c*) T. Newhouse, P. S. Baran and R. W. Hoffmann, The economies of synthesis, *Chem. Soc. Rev.*, 2009, **38**, 3010–3021.

3 I. P. Beletskaya, C. Nájera and M. Yus, Chemodivergent Reactions, *Chem. Soc. Rev.*, 2020, **49**, 7101–7166.

4 For selected reviews, see: (*a*) M. Font, M. Gulías and J. L. Mascareñas, Transition-Metal-Catalyzed Annulations Involving the Activation of C(sp^3)–H Bonds, *Angew. Chem., Int. Ed.*, 2022, **61**, e202112848; (*b*) M. Gulías and J. L. Mascareñas, Metal-Catalyzed Annulations through Activation of C–H Bonds: Recent Advances, *Angew. Chem., Int. Ed.*, 2016, **55**, 11000–11019.

5 B. Liu, A. M. Romine, C. Z. Rubel, K. M. Engle and B. F. Shi, Transition-Metal-Catalyzed, Coordination-Assisted Functionalization of Nonactivated C(sp^3)–H Bonds, *Chem. Rev.*, 2021, **121**, 14957–15074.

6 (*a*) R. S. Thombal, P. Y. M. Rubio, D. Lee, D. Maiti and Y. R. Lee, Modern Palladium-Catalyzed Transformations Involving C–H Activation and Subsequent Annulation, *ACS Catal.*, 2022, **12**, 5217–5230; (*b*) O. Baudoin, Ring Construction by Palladium(0)-Catalyzed C(sp^3)–H Activation, *Acc. Chem. Res.*, 2017, **50**, 1114–1123.

7 (*a*) A. García-Viada, J. C. Carretero, J. Adrio and N. Rodríguez, Insights into the mechanism of 3d transition-metal-catalyzed directed C(sp^3)–H bond functionalization reactions, *Chem. Soc. Rev.*, 2025, **54**, 4353–4390; (*b*) T. Dalton, T. Faber and F. Glorius, C–H Activation: Toward Sustainability and Applications, *ACS Cent. Sci.*, 2021, **7**, 245–261; (*c*) P. Gandeepan, T. Müller, D. Zell, G. Cera, S. Warratz and L. Ackermann, 3d Transition Metals for C–H Activation, *Chem. Rev.*, 2019, **119**, 2192–2452.

8 A. A. Mishra, D. Subhedar and B. M. Bhanage, Cobalt and Palladium Catalysed C–H Functionalization of Unactivated C(sp^3)–H Bond, *Chem. Rec.*, 2019, **19**, 1829–1857.

9 For selected reviews, see: (*a*) T. Yang, Y. Zhang, Y. Dou, D. Yang and J.-L. Niu, Earth-abundant cobalt-catalyzed enantioselective C–H functionalizations, *Sci. China: Chem.*, 2026, **69**, 659–679; (*b*) B. Desai, A. Uppuluru, A. Dey, N. Deshpande, B. Z. Dholakiya, A. Sivaramakrishna, T. Naveen and K. Padala, The recent advances in cobalt-catalyzed C(sp^3)–H functionalization reactions, *Org. Biomol. Chem.*, 2023, **21**, 673–699; (*c*) Y. Zheng, C. Zheng, Q. Gu and S. L. You, Enantioselective C–H functionalization reactions enabled by cobalt catalysis, *Chem. Catal.*, 2022, **2**, 2965–2985; (*d*) R. Mei, U. Dhawa, R. C. Samanta, W. Ma, J. Wencel-Delord and L. Ackermann, Cobalt-Catalyzed Oxidative C–H Activation: Strategies and Concepts, *ChemSusChem*, 2020, **13**, 3306–3356; (*e*) Y. Liu, T. You, H. X. Wang, Z. Tang, C. Y. Zhou and C. M. Che, Iron- and cobalt-catalyzed C(sp^3)–H bond functionalization reactions and their application in organic synthesis, *Chem. Soc. Rev.*, 2020, **49**, 5310–5358; (*f*) A. Baccalini, S. Vergura, P. Dolui, G. Zanoni and D. Maiti, Recent advances in cobalt-catalyzed C–H functionalizations, *Org. Biomol. Chem.*, 2019, **17**, 10119–10141; (*g*) T. Yoshino and S. Matsunaga, Cobalt-Catalyzed C(sp^3)–H Functionalization Reactions, *Asian J. Org. Chem.*, 2018, **7**, 1193–1205; (*h*) Y. Kommagalla and N. Chatani, Cobalt(II)-catalyzed C–H bond functionalization using an *N*,*N*′-bidentate directing group, *Coord. Chem. Rev.*, 2017, **350**, 117–135; (*i*) M. Usman, Z. H. Ren, Y. Y. Wang and Z. H. Guan, Developments in Cobalt Catalyzed Carbon–Carbon and Carbon–Heteroatom Bond Formation via C–H Bond Functionalization, *Synthesis*, 2017, 1419–1443; (*j*) M. Moselage, J. Li and L. Ackermann, Cobalt-Catalyzed C–H Activation, *ACS Catal.*, 2016, **6**, 498–525.

10 (*a*) L. Lukasevics, A. Cizikovs and L. Grigorjeva, C–H bond functionalization by high-valent cobalt catalysis: current progress, challenges and future perspectives, *Chem. Commun.*, 2021, **57**, 10827–10841; (*b*) P. G. Chirila and C. J. Whiteoak, Recent advances using [Cp*Co(CO)I_2] catalysts as a powerful tool for C–H functionalization, *Dalton Trans.*, 2017, **46**, 9721–9739; (*c*) S. Wang, S. Y. Chen and X. Q. Yu, C–H functionalization by high-valent Cp*CoIII catalysis, *Chem. Commun.*, 2017, **53**, 3165–3180; (*d*) T. Yoshino and S. Matsunaga, (Pentamethylcyclopentadienyl)cobalt(III)-Catalyzed C–H Bond Functionalization: From Discovery to Unique Reactivity and Selectivity, *Adv. Synth. Catal.*, 2017, **359**, 1245–1262.

11 (*a*) X. Wu, K. Yang, Y. Zhao, H. Sun, G. Li and H. Ge, Cobalt-catalyzed site-selective intra- and intermolecular dehydrogenative amination of unactivated sp^3 carbons, *Nat. Commun.*, 2015, **6**, 6462–6471; For elegant examples using directing groups distinct from 8-AQ, see: (*b*) H. Zhang, M.-C. Sun, D. Yang, T. Li, M.-P. Song and J.-L. Niu, Cobalt(II)-catalyzed activation of C(sp^3)–H bonds: organic oxidant-enabled selective functionalization, *ACS Catal.*, 2022, **12**, 1650–1656; (*c*) H. Zhang, D. Yang, X.-F. Zhao, J.-L. Niu and M.-P. Song, Cobalt-catalyzed C(sp^3)–H bond functionalization to access indole derivatives, *Org. Chem. Front.*, 2022, **9**, 3723–3729.

12 Z. Z. Zhang, Y. Q. Han, B. B. Zhan, S. Wang and B. F. Shi, Synthesis of Bicyclo[n.1.0]alkanes by a Cobalt-Catalyzed Multiple C(sp^3)–H Activation Strategy, *Angew. Chem., Int. Ed.*, 2017, **56**, 13145–13149.

13 (*a*) A. Garcia-Viada, E. Duro, C. Sánchez-González, I. Alonso, N. Rodríguez, J. Adrio and J. C. Carretero, Ag/Co-Bimetallic Cooperation in the C–H Functionalization of Aliphatic Amides with Propiolic Acids, *ACS Catal.*, 2025, **15**, 148–155; (*b*) J. Zhang, H. Chen, C. Lin, Z. Liu, C. Wang and Y. Zhang, Cobalt-Catalyzed Cyclization of Aliphatic Amides and Terminal Alkynes with Silver-Cocatalyst, *J. Am. Chem. Soc.*, 2015, **137**, 12990–12996.

14 (*a*) N. Barsu, D. Kalsi and B. Sundararaju, Site-selective C–H bond carbonylation with CO_2 and cobalt-catalysis, *Catal. Sci. Technol.*, 2018, **8**, 5963–5969; (*b*) P. Williamson, A. Ga and M. J. Gaunt, Cobalt-catalyzed C–H carbonylative cyclisation of aliphatic amides, *Chem. Sci.*, 2017, **8**, 2588–2591; (*c*) L. Zeng, S. Tang, D. Wang, Y. Deng, J. L. Chen, J. F. Lee and A. Lei, Cobalt-Catalyzed Intramolecular Oxidative C(sp^3)–H/N–H Carbonylation of Aliphatic Amides, *Org. Lett.*, 2017, **19**, 2170–2173; (*d*) N. Barsu, S. K. Bolli and B. Sundararaju, Cobalt catalyzed carbonylation of unactivated C(sp^3)–H bonds, *Chem. Sci.*, 2017, **8**, 2431–2435.

15 (*a*) M. Aslam, M. S. Akhtar, H. N. Lim, J. H. Seo and Y. R. Lee, Recent Advances in the Transformation of Maleimides *via* Annulation, *Org. Biomol. Chem.*, 2025, **23**, 269–291; (*b*) R. Manoharan and M. Jeganmohan, Alkylation, Annulation, and Alkenylation of Organic Molecules with Maleimides by Transition-Metal-Catalyzed C–H Bond Activation, *Asian J. Org. Chem.*, 2019, **8**, 1949–1969.

16 S. L. Liu, C. Ye and X. Wang, Recent Advances in Transition-Metal-Catalyzed Directed C–H Alkenylation with Maleimides, *Org. Biomol. Chem.*, 2022, **20**, 4837–4845.

17 (*a*) S. L. Liu, Y. Shi, C. Xue, L. Zhang, L. Zhou and M. P. Song, Maleimides in Directing-Group-Controlled Transition-Metal-Catalyzed Selective C–H Alkylation, *Eur. J. Org. Chem.*, 2021, 5862–5879; For an elegant example, see: (*b*) F. Lu, Y. Geng, H. Wang, Y.-N. Liu, E. Zhang, L. Yang and J. Tang, Late-stage modification of peptides with maleimides through palladium-catalyzed β-C (sp^3)–H alkylation, *Org. Lett.*, 2024, **26**, 8786–8791.

18 For some selected examples using noble metal catalysis, see: (*a*) V. Kumaria and L. H. Choudhury, Perimidine directed Rh(III)-catalyzed [4 + 1] and [4 + 2] annulations: synthesis of perimidine linked spiro-succinimides and isoquinolines, *Org. Chem. Front.*, 2026, **13**, 455–461; (*b*) S. Yang, X. Zuoa and Y. Zhang, Palladium-catalyzed three-component annulation reaction involving multiple C–H activation, *Org. Chem. Front.*, 2025, **12**, 1177–1182; (*c*) L. Liu, Y. Liu, S. Li, J. Gao, J. Li and J. Wei, Rh(III)-Catalyzed [4 + 1] Annulation of Sulfoximines with Maleimides: Access to Benzoisothiazole Spiropyrrolidinediones, *J. Org. Chem.*, 2023, **88**, 3626–3635; (*d*) A. Kumar and K. R. Prabhu, Rhodium(III)-catalyzed [5 + 1] annulation of 2-alkenylphenols with maleimides: access to highly functionalized spirocyclic skeletons, *Chem. Commun.*, 2021, **57**, 8194–8197.

19 R. Manoharan and M. Jeganmohan, Cobalt-Catalyzed Oxidative Cyclization of Benzamides with Maleimides: Synthesis of Isoindolone Spirosuccinimides, *Org. Lett.*, 2017, **19**, 5884–5887.

20 W. K. Yuan and B. F. Shi, Synthesis of Chiral Spirolactams *via* Sequential C–H Olefination/Asymmetric [4 + 1] Spirocyclization under a Simple CoII/Chiral Spiro Phosphoric Acid Binary System, *Angew. Chem., Int. Ed.*, 2021, **60**, 23187–23192.

21 (*a*) T. von Münchow, S. Dana, Y. Xu, B. Yuan and L. Ackermann, Enantioselective electrochemical cobalt-catalyzed aryl C–H activation reactions, *Science*, 2023, **379**, 1036–1042; (*b*) C. Sen, B. Sarvaiya, S. Sarkar and S. C. Ghosh, Room-Temperature Synthesis of Isoindolone Spirosuccinimides: Merger of Visible-Light Photocatalysis and Cobalt-Catalyzed C–H Activation, *J. Org. Chem.*, 2020, **85**, 15287–15304.

22 (*a*) A. Dutta and M. Jeganmohan, Palladium-Catalyzed Aerobic Oxidative Spirocyclization of Alkyl Amides with Maleimides via β-C(sp^3)–H Activation, *Org. Lett.*, 2023, **25**, 6305–6310; For a recent contribution, see: (*b*) T. Chakraborty and M. Jeganmohan, Palladium-catalysed spiro-cyclisation of substituted amino acids with maleimides via γ-C(sp^3)–H bond activation, *Org. Lett.*, 2025, **27**, 3521–3526.

23 H. Park and J. Q. Yu, Palladium-Catalyzed [3 + 2] Cycloaddition via Twofold 1,3-C(sp^3)–H Activation, *J. Am. Chem. Soc.*, 2020, **142**, 16552–16556.

24 For selected examples of dual C–H, involving a C(sp^2)–H and a C(sp^3)–H bond, see: (*a*) T. Chakraborty and M. Jeganmohan, Palladium(II)-catalyzed [3 + 2] annulation of aromatic triflamides via maleimide-relayed dual C–H activation process, *Org. Lett.*, 2025, **27**, 13009–13014; (*b*) S. Mandal, M. Barman, B. Debnath and T. Punniyamurthy, Dual C(sp^3)–H and C(sp^2)–H Activation of 8-Methylquinoline N-Oxides: A Route to Access C7–H Bond, *Org. Lett.*, 2024, **26**, 7560–7564; (*c*) G. Naskar and M. Jeganmohan, Pd(II)-catalyzed cyclization of 2-methyl aromatic ketones with maleimides through weak chelation assisted dual C–H activation, *Chem. Commun.*, 2024, **60**, 6284–6287; (*d*) G. Naskar and M. Jeganmohan, Palladium-Catalyzed [3 + 2] Annulation of Aromatic Amides with

Maleimides through Dual C–H Activation, *Org. Lett.*, 2023, **25**, 2190–2195; (*e*) G. Naskar and M. Jeganmohan, Ligand-Enabled [3 + 2] Annulation of Aromatic Acids with Maleimides by C(sp^3)–H and C(sp^2)–H Bond Activation, *Chem. – Eur. J.*, 2022, **28**, e20220077; (*f*) Q. He and N. Chatani, Palladium-Catalyzed Site-Selective [3 + 2] Annulation via Benzylic and *meta*-C–H Bond Activation, *Angew. Chem., Int. Ed.*, 2021, **60**, 5189–5192; (*g*) W. X. Wei, M. Czajkowski, Y. Kuang, T. A. V. Nguyen, B. Qin and M. Tomanik, Palladium-Catalyzed Annulations *via* Sequential C–H Activations of C(sp^2)–H/C(sp^3)–H or C(sp^3)–H/C(sp^3)–H Bonds, *ACS Catal.*, 2024, **14**, 6535–6546.

25 In this system, replacement of $Co(OAc)_2{\cdot}4\ H_2O$ for the reaction of **1a** with anhydrous $Co(OAc)_2$ resulted in a decreased yield of 46% (see Table S1).

26 Possibly, the coordination of 8Q with cobalt defines the stereospecificity in the enolization/deuteration of the α position with respect to the carbonyl of the maleimide.

27 Y. Wang, C. Du, Y. Wang, X. Guo, L. Fang, M. P. Song, J. L. Niu and D. Wei, High-Valent Cobalt-Catalyzed C–H Activation/Annulation of 2-Benzamidopyridine 1-Oxide with Terminal Alkyne: A Combined Theoretical and Experimental Study, *Adv. Synth. Catal.*, 2018, **360**, 2668–2677.

28 The opposite arrangement of maleimide, as well as use of pivalate as ligand or anionic complexes resulted less favorable (see Fig. S3).

29 All attempts to find the triplet transition state corresponding to the 1,2-migratory insertion of the double bond into the N–Co bond were unsuccessful, evolving toward IM4-t.

30 This assessment is illustrated in the scheme below, where the Me groups have been distinguished, with one highlighted in blue:

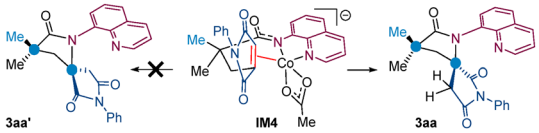

31 The *trans* relationship between the imide and the DG in **4aa′** agrees with the most stable transition state (TS1) found for the 1,2-migratory insertion of maleimide. The required insertion with the opposite orientation of maleimide to form **4aa** resulted to be less favorable (see Fig. S3).